HHS Public Access

Author manuscript

Matrix Biol. Author manuscript; available in PMC 2021 January 01.

Published in final edited form as:

Matrix Biol. 2020 January ; 85-86: 80–93. doi:10.1016/j.matbio.2019.07.006.

Scaffold stiffness influences breast cancer cell invasion via EGFR-linked Mena upregulation and matrix remodeling

Anthony J. Berger[a], **Carine M. Renner**[a], **Isaac Hale**[a], **Xinhai Yang**[a], **Suzanne M. Ponik**[b,c], **Paul S. Weisman**[c,d], **Kristyn S. Masters**[a,c,e,f,*], **Pamela K. Kreeger**[a,b,c,g,*]

[a]Department of Biomedical Engineering, University of Wisconsin-Madison, Madison, WI

[b]Department of Cell and Regenerative Biology, University of Wisconsin School of Medicine and Public Health, Madison, WI

[c]Carbone Cancer Center, University of Wisconsin School of Medicine and Public Health, Madison, WI

[d]Department of Pathology, University of Wisconsin School of Medicine and Public Health, Madison, WI

[e]Department of Medicine, University of Wisconsin School of Medicine and Public Health, Madison, WI

[f]Department of Materials Science and Engineering, University of Wisconsin-Madison, Madison, WI

[g]Department of Obstetrics and Gynecology, University of Wisconsin School of Medicine and Public Health, Madison, WI

Abstract

Clinically, increased breast tumor stiffness is associated with metastasis and poorer outcomes. Yet, *in vitro* studies of tumor cells in 3D scaffolds have found decreased invasion in stiffer environments. To resolve this apparent contradiction, MDA-MB-231 breast tumor spheroids were embedded in ‘low’ (2 kPa) and ‘high’ (12 kPa) stiffness 3D hydrogels comprised of methacrylated gelatin/collagen I, a material that allows for physiologically-relevant changes in stiffness while matrix density is held constant. Cells in high stiffness materials exhibited delayed invasion, but more abundant actin-enriched protrusions, compared to those in low stiffness. We find that cells in high stiffness had increased expression of Mena, an invadopodia protein associated with metastasis in breast cancer, as a result of EGFR and PLCγ1 activation. As invadopodia promote invasion

*Corresponding Authors: Pamela K. Kreeger (PKK), kreeger@wisc.edu, 1111 Highland Ave., 4553 WIMR II, Madison, WI 53705; Kristyn S. Masters (KSM), kmasters@wisc.edu, 1111 Highland Ave., 8531 WIMR II, Madison, WI 53705.

8. Authors’ contribution

AJB, KSM, and PKK conceived and designed the study. AJB, CMR, IH, XY, and SMP performed the experiments. AJB, CMR, SMP, PSW, and PKK analyzed the data. AJB, KSM, and PKK wrote the manuscript with input from all authors.

6. Declarations of interest

The authors declare no competing interests.

through matrix remodeling, we examined matrix organization and determined that spheroids in high stiffness displayed a large fibronectin halo. Interestingly, this halo did not result from increased fibronectin production, but rather from Mena/α5 integrin dependent organization. In high stiffness environments, *FN1* knockout inhibited invasion while addition of exogenous cellular fibronectin lessened the invasion delay. Analysis of fibronectin isoforms demonstrated that EDA-fibronectin promoted invasion and that clinical invasive breast cancer specimens displayed elevated EDA-fibronectin. Combined, our data support a mechanism by which breast cancer cells respond to stiffness and render the environment conducive to invasion. More broadly, these findings provide important insight on the roles of matrix stiffness, composition, and organization in promoting tumor invasion.

Keywords

tumor microenvironment; extracellular matrix; biomaterials

1. Introduction

The breast tumor microenvironment can alter cell behavior via myriad extracellular cues, ranging from soluble factors secreted by the resident cells [1] to the physical properties of the extracellular matrix (ECM) itself [2, 3]. During the progression from normal to pathological ECM in breast cancer, fibrous proteins, such as collagen and fibronectin, are deposited, reorganized, and crosslinked [4–6], leading to significant alterations in tissue mechanics [7, 8]. The aberrant collagen alignment and increased tissue rigidity found in primary breast tumors have each been shown to correlate with a more aggressive phenotype and poor patient survival [7, 9–11]. Similarly, altering ECM organization in mouse models of breast cancer by either inhibiting [12, 13] or enhancing [14] fiber formation, which simultaneously affects tissue stiffness, has demonstrated a link between cancer cell invasion and the physical properties of the ECM. Because ECM density, fibrosity, and stiffness are all coupled, determining the individual impact of these different physical cues can be difficult in *in vivo* systems.

In vitro platforms offer substantially better control over matrix properties, allowing for the investigation of how specific ECM characteristics affect different cell behaviors. For instance, *in vitro* platforms have been widely used to establish that changes in biomolecule presentation within an ECM can have profound effects on intracellular signaling [15]. Unfortunately, many *in vitro* systems capable of decoupling scaffold stiffness and ECM density are unable to accurately recapitulate important aspects of the disease microenvironment. For example, collagen gels can be stiffened independent of changes in collagen density via crosslinking with reactive PEG moieties. Such hydrogel systems have been used to demonstrate that increased stiffness yields higher breast cancer invasion rates [16]. However, the achievable range of elastic moduli was limited to under 1 kPa, while the breast cancer microenvironment reaches stiffnesses of greater than 10 kPa [7]. Other scaffold materials, such as photopolymerizable PEG or gelatin-methacrylate, can be fabricated at a wide range of elastic moduli but do not provide a physiologically relevant fibrous

topography, an ECM attribute that is critical to tumor progression *in vivo* [17] and required for invasion for some breast cancer subtypes *in vitro* [18].

To address these limitations, we have recently developed an interpenetrating network of collagen I and gelatin-methacrylate [19]. With this hydrogel system, scaffold stiffness can be altered over a wide range (2–12 kPa) while maintaining a fibrous topography and equivalent ECM density. Consistent with patient data supporting a relationship between collagen organization and poor prognosis [9], we found that MDA-MB-231 breast cancer cells required collagen fibers in order to invade [19]. However, while stiffer tumors are associated with increased metastatic behavior and poor prognosis [7, 20], our previous results demonstrated that increasing scaffold stiffness decreased invasion. To reconcile this contradiction, the present work sought to further examine how increased matrix rigidity influenced cell invasion over time and identify mechanisms by which tumor cells overcome this initial resistance.

2. Materials and Methods

2.1 Materials and Cell Culture

Unless otherwise noted, all chemicals were purchased from Sigma-Aldrich (St. Louis, MO). MDA-MB-231 human triple-negative breast cancer cells (ATCC, Manassas, VA) were used until passage 25. MDA-MB-231 cells were maintained at 37°C and 5% CO_2 in DMEM (Corning, Corning, NY) supplemented with 10% Hyclone fetal bovine serum (FBS, Thermo Scientific, Logan, UT), 100 U/mL penicillin-streptomycin, and 2 mM L-glutamine.

2.2 Gelatin Methacrylation

GelMA was synthesized as described previously [19]. Briefly, type-A porcine skin gelatin was dissolved at 10% w/v in phosphate buffered saline (PBS) at 50°C. Methacrylic anhydride (MA) was added to the gelatin solution using a peristaltic pump at a rate of 200 μL/min under aggressive stirring. Final MA concentrations of 0.25 and 7% v/v were used and will be referred to as 0.25M and 7M herein. The reaction proceeded for 24 hours at 50°C shielded from light, after which it was spun down at 3000×g for 5 minutes to pellet unreacted MA and precipitated protein. The supernatant was dialyzed against PBS using 12–14 kDa MWCO dialysis tubing (Spectrum Labs, Rancho Dominguez, CA) for 2 days at 50°C, at which point the dialysis solution was switched to ddH_2O for another 3 days at 50°C. Dialysis buffer was changed daily during dialysis. The gelMA solution was filtered, lyophilized, and stored at −20°C.

2.3 GelMA/Collagen Hydrogel Preparation

Hydrogels were generated as previously described [19]. Briefly, gelMA was resuspended at 20% w/v in DMEM (Corning, Corning, NY) without serum or phenol red and incubated in a 50°C water bath until dissolved. The 0.25M and 7M gelMA modifications were tuned to produce two different gel stiffness conditions (a low 2 kPa and high 12 kPa). The gelMA solution was then combined with the photoinitiator lithium phenyl-2,4,6-trimethylbenzoylphosphinate (LAP; 0.05% w/v final concentration) [21], serum-free phenol red-free DMEM, and 10X PBS in a 37°C water bath. Directly before photopolymerization,

native bovine collagen type 1 (Fibricol, Advanced Biomatrix, San Diego, CA) was added to the prepolymer solution, which was then vortexed and spun down to remove bubbles. The gelMA was photocrosslinked via UV exposure at 365 nm (3.4 mW/cm^2) for 4 minutes at 37°C.

Hydrogel swelling behavior was measured as percent increase in wet weight after a 24 hour incubation at 37°C in PBS, and an iterative process was followed to modify the starting prepolymer formulations in order to achieve a final, post-swelling concentration of 5% gelMA across all conditions. Specifically, the initial gelMA concentrations were 5% and 7.2% for high and low stiffness, respectively, which yielded a final post-swelling gelMA concentration of 5% in both conditions. A similar procedure was used to determine the initial collagen concentrations required to yield gels with a post-swelling collagen concentration of 1.5 mg/mL. As shown in Table S1, 1.5 and 2.16 mg/mL collagen were used for high and low stiffness gels, respectively, to yield a final concentration of 1.5 mg/mL. Example formulations for 1 mL prepolymer of each condition are listed in Table S1.

In experiments that incorporated exogenous cellular fibronectin (cFN, isolated from human foreskin fibroblasts, Sigma-Aldrich), the protein was added to the prepolymer solution to achieve a final concentration of 25 μg/mL and briefly vortexed directly before the addition of collagen. The volume of fibronectin added was accounted for in the formulation by adjusting the volume of DMEM.

2.4 Tumor Spheroid Fabrication

MDA-MB-231 cell cultures were detached with TrypLE (Thermo Fisher Scientific, Waltham, MA) to generate a single-cell suspension and diluted to 40,000 cells/mL in ice-cold growth medium. A volume of 50 μL was then added to each well of a 96-well v-bottom plate (Corning, Corning, NY). To prevent cell attachment, the plate was previously coated with 50 μL/well 1% Poly-HEMA in 95% ethanol and air dried at 37°C overnight in a biological safety cabinet. The cells were pelleted into the v-bottom of each well by centrifugation at 1000×g for 10 minutes at 4°C using an Eppendorf 5810R centrifuge (Eppendorf, New York, NY). After centrifugation, 50 μL of ice cold growth medium supplemented with 0.35 mg/mL Matrigel (BD Biosciences, San Jose, CA) was gently layered over each well. The plate was then incubated under standard culture conditions for 24 hours, yielding spheroids with an average diameter of 150–200 μm.

2.5 Spheroid Invasion Assay

Spheroids were collected, centrifuged at 500×g, and resuspended in serum-free, phenol red-free DMEM. The spheroid solution was then placed on a rotating platform and incubated at 4°C for 20 minutes to remove any residual FBS and Matrigel. This process was repeated three times. For α5 integrin blocking experiments, spheroids were placed in a solution of anti-α5 integrin antibody (Clone P1D6, 1:100 dilution, Mouse, Abcam, cat# ab78614, Cambridge, MA) in serum-free, phenol-red free DMEM and incubated on a rotating platform for one hour directly before embedding.

The spheroid solution was combined with gelMA/collagen prepolymer to yield a final concentration of 10 spheroids/50 μL of hydrogel solution. The solution was distributed into a

96-well angiogenesis μ-plate (Ibidi, Fitchburg, WI) at 10 μL per well, and hydrogel polymerization was performed as described above. Gels were then fed with serum-free DMEM or serum-free DMEM supplemented with 50 μM irigenin (blocks binding of α integrins to the EDA loop of EDA-fibronectin, Ark Pharm, Arlington Heights, IL), 10 μM gefitinib (EGFR inhibitor, Selleck Chem, Houston, TX), 10 μM GM6001 (pan-MMP inhibitor, Selleck Chem), or 5 μM U73122 (PLCγ1 inhibitor, Tocris, Minneapolis, MN). At 12, 24, 48, and/or 72 hours post-encapsulation, spheroids were fixed with 10% formalin and permeabilized with 0.25% Triton-X. Cell nuclei were stained with DAPI (0.3 μM) in PBS with 1% BSA. Gels were washed with PBS and imaged on a Leica SP8 confocal microscope (Leica, Buffalo Grove, IL). Z-stacks spanning 150 μm around the spheroid were taken utilizing either a Leica 10X Plan Apo Dry 0.4 NA or a 20X Plan Apo Dry 0.75 NA objective and orthogonally projected in the z-direction to generate 2D images for analysis. The images were converted to binary and the 'analyze particles' tool in FIJI imaging software [22] was utilized to count the number of nuclei that had separated from the spheroid body (n=12–32 spheroids per condition). The mean number of invading cells and standard deviation can be found for each experimental condition in Table S2.

2.6 Immunofluorescent Staining in GelMA/Collagen gels

Spheroid invasion assays were performed as described above. At 12, 24, 48, and/or 72 hours, gels were fixed with 10% formalin and, for intracellular targets, cells were permeabilized with 0.25% Triton-X. A solution of 5% BSA in PBS was used to block the gels for 24 hours at 37°C. Gels were incubated for 48 hours at 37°C with the appropriate primary antibody: anti-plasma fibronectin (Cat# ab2414; 1:100, Rabbit, Abcam), anti-EDA-fibronectin (Cat# ab6328; 1:100, Mouse, Clone IST9, Abcam), anti-Mena (Cat# 610693; 1:50, Mouse, Clone 21, BD Biosciences), or pPLCγ1 (Cat# 44–696G; Tyr783, 1:100, Rabbit, Thermo Fisher Scientific). Unbound primary antibody was removed via four 30 minute washes with PBS (1:4 ratio gel volume:PBS) at 37°C. Gels were incubated with secondary antibodies, either goat anti-mouse IgG conjugated to Alexa 488 or goat anti-rabbit IgG conjugated to Alexa 564 (1:200, Invitrogen, Grand Island, NY) in PBS with 1% BSA, for 24 hours at 37°C. Gels were again washed thoroughly with PBS, stained with DAPI, and imaged by confocal microscopy as described above. Mean fluorescent intensities for confocal images are quantified in Figure S1.

2.7 Multiphoton Imaging

Samples were imaged on a multiphoton microscope consisting of a Nikon TE300 inverted base, a Coherent Chameleon XR laser path, and Hamamatsu H7422P-40 photomultiplier. Cell autofluorescence (FAD) was collected using a laser excitation of 890 nm with emission filtration using a Semrock Brightline® 445/20 nm filter. Fibronectin immunofluorescence was visualized with an Alexa-488 secondary antibody, excited at 890 nm with emission filtration using a Semrock Brightline® 520/35 nm filter. Spheroids were imaged as a z-series with 2 μm step-size using a Nikon CFI Apo λS 40X 1.25-NA water immersion objective.

2.8 RNA Isolation and qRT-PCR on Tumor Spheroids in GelMA/Collagen gels

For RNA isolation, spheroids were generated and collected as above. After combining with the prepolymer solution to yield a final concentration of 10 spheroids/50 μL prepolymer, the

solution was distributed into a 96-well plate at 75 μL per well, and hydrogel polymerization was performed as described. At 12, 24, 48, or 72 hours, gels were digested in a 1:1 volume of 6 mg/mL Proteinase K (Qiagen, Germantown, MD), 5X trypsin, and 4 mg/mL collagenase type 2 (Worthington, Columbus, OH) for 25 minutes at 37°C. A total of three gels were pooled for each replicate, and RLT buffer was added to the digests, at which point the solutions were incubated for another 30 minutes in a 50°C water bath to complete the digestion of the gels. RNA isolation was performed using micro-RNeasy spin columns (Qiagen), and cDNA was synthesized using the High-Capacity cDNA Reverse Transcription kit (Thermo Fisher Scientific). qRT-PCR was performed using primers for *EGFR, FN1, HSPB90AA, HSPB90AB, ENAH* (Qiagen), *MENA-INV* (Forward Primer: GATTCAAGACCATCAGGTTGTG, Reverse Primer: TACATCGCAAATTAGTGCTGTC, [23]), and *EDA-FN1* (Forward Primer: GGAGAGAGTCAGCCTCTGGTTCAG, Reverse Primer: TCTGCAGTGTCTTCTTCACC [24]) with SsoAdvanced Universal SYBR Green Supermix (Bio-Rad, Hercules, CA). Fold change was calculated using the ddCT method with *GAPDH* as the reference gene. Three samples from each condition were run in duplicate.

2.9 siRNA Knockdown in MDA-MB-231 Spheroids

To knockdown *FN1* and *ENAH*, MDA-MB-231 cells were seeded in complete growth media at 75,000 cells/cm^2 in a six-well plate and allowed to adhere overnight. Cells were then treated for 24 hours with 25 nmol/L SMARTpool, targeted to either *FN1* or *ENAH*, or non-targeting pooled siRNA (Dharmacon, Lafayette, CO) in complete growth media without penicillin/streptomycin. After treatment, cells were washed with PBS and used to generate spheroids as above.

2.10 Immunostaining of Breast Tumor Microarray

The breast carcinoma tissue microarray (TMA) was obtained from the University of Wisconsin Carbone Cancer Center BioBank. The construction of the TMA with deidentified patient tissue and select clinical patient information with a waiver of consent was approved by the University of Wisconsin Institutional Review Board (OS10111). The TMA included samples of benign tissue, ductal carcinoma *in situ* (DCIS), and four categories of invasive breast cancer: estrogen or progesterone receptor-positive/HER2-negative (ER/PR+), estrogen or progesterone receptor-negative/HER2-positive (HER2+), triple negative breast cancer (TNBC), and triple positive breast cancer (TPBC). Classification as DCIS or invasive on the TMA sample was confirmed by a blinded pathologist. For staining, 5 μm sections of the TMA were deparaffinized using SafeClear II (Thermo Scientific) and rehydrated using a series of graded ethanol washes (100, 95, 70, and 50%) followed by a wash in water. Antigen retrieval was performed using a citric acid-based unmasking solution (Vector Laboratories, Burlingame, CA) with microwaving at high power until the solution reached boiling point, then at 20% power for 15 minutes longer. Slides were blocked overnight at 4°C using blocking serum from VECTASTAIN ABC/HRP Universal Staining Kit following manufacturer's instructions (Vector Laboratories).

Primary antibodies used were FN-EDA (Clone IST9, 1:50, 2 hours, Abcam) and pan-cytokeratin (Cat# ab9377; 1:200, 2hrs, Abcam) and secondary antibodies were Alexa Fluor

647 goat anti-rabbit and Alexa Fluor 488 goat anti-mouse (both 1:200, 1hr, Thermo Scientific). The TMA was counterstained and mounted with ProLong Diamond Antifade Mountant with DAPI (ThermoFisher). Each core was imaged using a Zeiss Axio Observer.Z1 inverted microscope with an AxioCam 506 mono camera, Plan-Apochromat 20× 0.8-NA air objective, and Zen2 software to tile images across each 0.6 mm sample (Zeiss, Oberkochen, Germany). The mean intensity of the FN-EDA was quantified in FIJI, with background levels from breast tumor samples stained only with secondary antibodies subtracted.

2.11 Statistics

Data were analyzed using one-way analysis of variance (ANOVA), Tukey's test, and Dunnett's test in Prism 7 (GraphPad Software, La Jolla, CA) with $p<0.05$ considered statistically significant. All values are expressed as mean +/− standard deviation.

3. Results and Discussion

3.1 Scaffold rigidity alters the invasive behavior of breast cancer cells

We have previously observed a decrease in MDA-MB-231 cell invasion at 72 hours with increasing scaffold stiffness [19]. To expand on these results, we first analyzed how the invasion kinetics of MDA-MB-231 spheroids embedded in low (2 kPa) and high (12 kPa) stiffness gelMA/Coll hydrogels differed over the course of 72 hours (Figure 1A). We noted significant invasion in the low stiffness condition occurring as early as 24 hours, but delayed invasion in the high stiffness gels, which showed little invasion activity during the first 48 hours of culture (Figure 1A,B). Furthermore, the rate of invasion was linear in low stiffness conditions, whereas spheroids embedded in stiffer gels underwent ~80% of their total invasion during the last 24 hours of the experiment (Figure 1C). Consistent with our previous work, the presence of collagen fibers was required for MDA-MB-231 invasion in a high stiffness environment, as 12 kPa scaffolds made from gelMA alone did not support invasion (Figure S2A).

The drastic differences in invasion kinetics raised the possibility of differences in the method of invasion. In proteolytically-independent invasion, cells apply force directly to the ECM and physically displace matrix fibrils; by adopting elongated or amoeboid-like shapes, movement through the dense matrix is then possible [25, 26]. In contrast, with proteolytic invasion, cell production of matrix metalloproteinases (MMPs) degrades the matrix, opening holes through which the cell can migrate [27]. Because cell morphology is often indicative of the mode of invasion, we examined this feature in low and high stiffness scaffolds. MDA-MB-231 cells in low stiffness scaffolds left the spheroid core as either long, symmetrical, spindle-like shapes or rounded, amoeboid cells (Figure 2A, left panel). In contrast, cells in high stiffness scaffolds were smaller and exhibited numerous long, thin actin-enriched protrusions that extended into the surrounding matrix (Figure 2B, center and right panel). These morphologies have been associated with proteolytically-independent and -dependent invasion, respectively [28]. Therefore, we next used GM6001, a pan-MMP inhibitor, to assess whether the differences in invasion between high and low stiffness conditions were related to proteolytic activity. Treatment with GM6001 decreased the number of invading

cells in 2 kPa gels, but did not stop invasion or alter cell morphologies (Figure 2B,C). However, in the 12 kPa condition, GM6001 inhibited the development of cellular protrusions and completely suppressed invasion (Figure 2B,C), suggesting that invasion was entirely proteolytically-dependent in the high stiffness environment.

3.2 Mena expression is upregulated in stiff hydrogels

We next sought to identify the mechanism responsible for the increased density of actin-enriched protrusions and onset of proteolytic invasion observed in high stiffness gels. As these observations are consistent with invadopodia, we considered the proteins involved in invadopodia maturation [29]. The actin regulatory protein Mena [30] was of particular interest as it is highly upregulated in invasive cancer cells collected from primary tumors [31] and involved in several motility pathways associated with invasive behavior [32]. Furthermore, high Mena levels are associated with a poor clinical outcome in breast cancer patients [33, 34]. Therefore, we examined the levels of Mena in the 2 and 12 kPa hydrogels. Substantially more Mena was observed in high stiffness gels at both early (12 hr) and late (72 hr) time points compared to low stiffness (Figure 3A). Mena expression was localized to the cells at the spheroid edge and those that had begun invading, consistent with a potential role in the observed invasion. In agreement with the lack of invasion in high stiffness gelMA scaffolds lacking fibrillar collagen, Mena was not detected in 12 kPa gelMA-only scaffolds (Figure S2B). At the mRNA level, the elevation in total *MENA* was relatively modest (Figure 3B); therefore, we examined expression of *MENA-INV*, a splice variant that imparts a more invasive phenotype in breast cancer cells [23]. In particular, *MENA-INV* is elevated in primary breast tumor cells capable of transendothelial migration [35] and elevated Mena-Calc (an indirect measurement of $Mena^{Inv}$) correlated with poor survival in breast cancer patients [36]. *MENA-INV* was found to be two-fold greater in 12 kPa gels, with upregulation starting as early as 12 hours post-embedding (Figure 3C). While previous work using mouse models and patient samples suggested that changing ECM stiffness could lead to an increase in $Mena^{INV}$ [37], ours is the first study to demonstrate a direct link, a finding only made possible through our hydrogel platform that decouples scaffold stiffness and ECM density while retaining fibrillar architecture. The role of Mena in stiffness-dependent invasion was further investigated via knockdown of *MENA* expression using siRNA (Figure S3). Consistent with the lack of actin-enriched protrusions and low Mena levels in 2 kPa gels, Mena knockdown had no effect on invasion in low stiffness gels (Figure 3D). In contrast, knocking down *MENA* reduced invasion in 12 kPa scaffolds by more than 65% (Figure 3D).

3.3 EGFR activation of PLCγ1 links ECM stiffness to Mena production

To identify the connection between increased scaffold stiffness and Mena upregulation, we examined the literature for known regulators of Mena. EGFR activation has been shown to be required for Mena activity in breast cancer cells *in vitro* [38] and cells on different stiffness substrates exhibit differential sensitivity to EGF ligands [39]. In our system, treatment with gefitinib, a reversible EGFR inhibitor, significantly reduced the spread and intensity of Mena staining in high stiffness gels and completely inhibited cell invasion (Figure 4A). As *EGFR* expression was unaffected by stiffness (Figure S4), we hypothesized that differences in post-translational signaling activity existed between soft and stiff

environments. While there are myriad signal mediators downstream of EGFR that could potentially influence Mena, we focused on AKT, which has previously been identified as a regulator of Mena [40], and PLCγ1, a phospholipase that plays a central role in invadopodia formation [41, 42] and is upregulated in breast tumors [43]. While pAKT levels did not appear to be affected by stiffness (Figure S5), pPLCγ1 was found to be more robust in high stiffness gels relative to low stiffness at both early (12 hr) and late (72 hr) time points, with a clear localization to the edge of the spheroid (Figure 4B). Additionally, treatment of spheroids in 12 kPa gels with gefitinib eliminated pPLCγ1 accumulation, indicating the increase in PLCγ1 activity was dependent on EGFR signaling (Figure S6).

Since pPLCγ1 staining mirrored Mena staining and the intensity of both were decreased significantly by EGFR inhibition, we hypothesized that stiffness-related EGFR activation led to PLCγ1 activation, which resulted in Mena upregulation. To test the link between PLCγ1 and Mena, spheroids in low and high stiffness gels were treated with the PLCγ1 inhibitor U71322 directly after embedding. Consistent with our hypothesis, Mena levels at 72 hours were considerably lower in samples treated with U71322 (Figure 4C, left panel) and invasion was significantly decreased in the high stiffness condition while unaffected in the low stiffness condition, where PLCγ1 activation and Mena expression are already low (Figure 4D). However, it is possible that PLCγ1 influences invasion independent of Mena expression. To test for this possibility, we analyzed the impact of PLCγ1 inhibition when initiated 24 hours after encapsulation, at which point Mena levels have already increased in high stiffness gels (Figure 3A). In this condition, Mena expression was preserved (Figure 4C, right panel) and invasion was unaffected in both low and high stiffnesses (Figure 4D). Combined, these results support that PLCγ1 phosphorylation is downstream of EGFR activation but upstream of Mena upregulation, and that Mena upregulation is essential for invasion in high stiffness conditions.

3.4 Increased Mena expression leads to extracellular deposition of fibronectin in stiff matrices via the α5 integrin

Mena, and Mena-INV in particular, not only regulate invadopodia formation and stability, but also influence binding to, haptotaxis on, and reorganization of extracellular fibronectin via association with the α5 integrin [44], and *ITGA5* expression has been previously shown to correlate with shorter overall survival in breast cancer [45]. Accordingly, we evaluated if the stiffness-dependent changes we observed in Mena expression impacted fibronectin deposition in the matrix surrounding the tumor spheroids. Interactions between fibronectin and collagen I have been shown to impact tumor growth, but prior studies have focused on the role of cancer-associated fibroblasts in remodeling the ECM [46], while our study incorporated only the epithelial component of the tumor. While spheroids in both conditions produced fibronectin, the staining intensity was dramatically increased in high stiffness gels and localized as a halo that spread from the spheroid (Figure 5A, raw fluorescent images Figure S7). The halo of fibronectin in 12 kPa scaffolds was observable as early as 24 hours and increased in size and intensity over the 72 hour experiment duration. Intriguingly, total fibronectin recovered from digested gels and *FN1* expression were similar between low and high stiffness conditions (Figure S8A), indicating the halo was not due to increased protein levels in stiff gels. Additionally, gene expression of chaperone proteins responsible for

shuttling fibronectin out of the cells was stiffness-dependent only at early times, before the halo was fully established (Figure S8B).

To evaluate if the fibronectin enrichment was due to the elevation in Mena in high stiffness gels, *MENA* was knocked down by siRNA, and the fibronectin halo was observed to nearly disappear (Figure 5B). Furthermore, treatment with an EGFR inhibitor similarly ablated the halo, while inhibitors of FAK and ROCK, common mediators in mechanosignaling [47], had no effect (Figure S9). Additionally, incubation of spheroids with an anti-α5 antibody to inhibit α5 integrin association with fibronectin reduced formation of the fibronectin halo (Figure 5C). While this result does not eliminate a potential role for other fibronectin-binding integrins in this process (*i.e.,* αvβ3, α4β1), the data support that Mena and α5 integrin help mediate the assembly and retention of the fibronectin halo.

3.5 EDA-fibronectin is upregulated in human breast tumors and critical to tumor spheroid invasion in stiff environments

Next, we set out to determine the effect of the fibronectin halo on breast cancer cell behavior. First, two-photon microscopy was used to obtain higher resolution imaging of fibronectin staining around the cancer spheroids. We observed increased fibronectin signal around invading cells (Figure 6A), suggesting the fibronectin is involved in tumor cell invasion. It has been demonstrated that deposition of fibronectin is necessary for fibroblast invasion in fibrin matrices [48]. To test the hypothesis that fibronectin is facilitating invasion in stiff matrices, we added cellular fibronectin, which has been observed in tumor microenvironments [49], to the gelMA scaffolds during polymerization. The addition of exogenous fibronectin doubled the total amount of spheroid invasion when added to high stiffness gels (Figure 6B). In low stiffness scaffolds, exogenous fibronectin did not change cell morphology (Figure S10A) or total invasion, indicating that fibronectin was essential for invasion only in the high stiffness environment. To confirm this finding, we next knocked down *FN1* by siRNA (Figure S10B). As expected, knockdown of fibronectin expression dramatically reduced both the intensity and spread of the fibronectin halo in both stiffnesses (Figure 6C). However, fibronectin knockdown affected cell invasion only in the high stiffness condition, where the total amount of cell invasion was decreased by two-fold (Figure 6D), while invasion in the low stiffness condition was unaltered.

Cellular fibronectin includes the EDA and EDB domains that are edited out of plasma fibronectin [50], and these domains have unique effects on cell behavior. To determine if the fibronectin halo included either of these domains, spheroids embedded in high stiffness hydrogels were stained for the two isoforms. While EDB-fibronectin staining levels were minimal (Figure S11A), our staining revealed the halo contained high levels of the EDA-fibronectin isoform (Figure 7A). Similar to our results for *FN1* expression, expression of *EDA-FN1* did not vary between soft and stiff environments (Figure S11B). EDA-fibronectin expression has been observed in invasive breast tumors [51], with more intense staining near the tumor's invasive edge [52] and *EDA-FN1* expression has been shown to be elevated in malignant cells cultured in 3D relative to benign cells [45]. Cells interact with the EDA domain of fibronectin via a protein loop in the EDA sequence that binds the α4 and α9 integrins [53]; elevated *ITGA9* expression in breast cancer is associated with early onset of

distant metastases and reduced overall survival [45]. EDA-fibronectin interactions with α4 and α9 can be disrupted by irigenin, a small molecule inhibitor that occupies the EDA protein loop and prevents integrins from binding to the EDA isoform [54]. Spheroids in high and low stiffness gels were treated with irigenin to investigate whether the EDA isoform specifically regulated tumor spheroid invasion. Blocking cellular interaction with EDA via irigenin treatment did not affect cellular morphology or total invasion in low stiffness conditions. However, the same treatment dramatically reduced formation of actin-enriched protrusions and cell invasion in high stiffness gels (Figure 7B,C).

Finally, we examined the *in vivo* relevance of these findings by determining whether invasive human breast tumors display increased levels of EDA-fibronectin. As *MENA-INV* levels are not correlated with hormone receptor/HER2 status [35], we elected to analyze a tumor microarray containing benign, ductal carcinoma in situ (DCIS, non-invasive), and invasive breast tumors (ER/PR+, HER2+, TNBC, and TPBC) for EDA-fibronectin (Figure 7D). EDA-fibronectin was observed in both the epithelial (pan-cytokeratin positive) and stromal fractions of tumors, consistent with prior reports of *FN1-EDA* expression by both tumor and stromal cells [51] and was present at significantly higher levels in invasive cancers of all subtypes compared to benign breast samples (Figure 7E). DCIS samples had an intermediate level of EDA-fibronectin relative to benign or invasive tumors, which did not reach statistical significance ($p=0.07$ relative to benign). Together with our *in vitro* results, these findings suggest that EDA-fibronectin may serve as a critical cue in the regulation of tumor cell invasion.

4. Conclusions

The present work illustrates a mechanism by which substrate stiffness can influence invasion behavior in breast cancer cells (Figure 7F). Increasing stiffness from low to high (2 to 12 kPa) led to a switch from proteolytically-independent invasion to a proteolytically-dependent phenotype. Increased deposition of fibronectin was observed around tumor spheroids in stiff scaffolds, which resulted from EGFR/PLCγ1 signaling that upregulated Mena expression and Mena-initiated fibronectin assembly via the α5 integrin. This local enrichment of fibronectin was largely composed of the EDA isoform, which was significantly upregulated in human breast cancer tissue samples when compared to benign tissues. Overall, these results demonstrate that, while microenvironmental cues such as stiffness may initially restrain tumor cell invasion, they can simultaneously activate intracellular signaling pathways by which tumor cells proceed to modify the microenvironment to a permissive state. Moreover, it is important to note that the novel, tunable interpenetrating fibrillar networks employed in this study were essential to revealing these mechanisms, as gelMA-only (non-fibrous) scaffolds failed to reproduce the invasion and Mena-centered behavior observed in stiff, gelMA/coll gels.

Supplementary Material

Refer to Web version on PubMed Central for supplementary material.

Acknowledgements

We thank the University of Wisconsin Carbone Cancer Center Optical Imaging Core and Translational Research Initiatives in Pathology Laboratory supported by NIH5P30CA014520.

7. Funding information

This work was supported by grants from the National Institutes of Health (1DP2CA195766 - PKK, 1R01CA232517 – PKK, KSM, 1R21CA202040 – PKK, KSM, 1R01CA179556 - SMP), the National Science Foundation (CBET-1401584 –KSM, PKK), the National Science Foundation Graduate Research Fellowship (AJB), and the Wisconsin Alumni Research Foundation (AJB).

Abbreviations

BSA	bovine serum albumin
cFN	cellular fibronectin
DCIS	ductal carcinoma in situ
ECM	extracellular matrix
EGFR	epidermal growth factor receptor
EMT	epithelial to mesenchymal transition
ER	estrogen receptor
FBS	fetal bovine serum
FN	Fibronectin
GelMA	gelatin methacrylate
HER2	epidermal growth factor receptor type 2
LAP	lithium phenyl-2,4,6-trimethylbenzoylphosphinate
MA	methacrylic anhydride
MMP	matrix metalloproteinase
PBS	phosphate buffered saline
PEG	polyethelene glycol
PLCγ	phospholipase C gamma
PR	progesterone receptor
TMA	tumor microarray
TNBC	triple negative breast cancer
TPBC	triple positive breast cancer

9. References

[1]. Witsch E, Sela M, Yarden Y, Roles for growth factors in cancer progression, Physiology (Bethesda) 25(2) (2010) 85–101. [PubMed: 20430953]

[2]. Jaalouk DE, Lammerding J, Mechanotransduction gone awry, Nat Rev Mol Cell Biol 10(1) (2009) 63–73. [PubMed: 19197333]

[3]. Butcher DT, Alliston T, Weaver VM, A tense situation: forcing tumour progression, Nat Rev Cancer 9(2) (2009) 108–22. [PubMed: 19165226]

[4]. Paszek MJ, Zahir N, Johnson KR, Lakins JN, Rozenberg GI, Gefen A, Reinhart-King CA, Margulies SS, Dembo M, Boettiger D, Hammer DA, Weaver VM, Tensional homeostasis and the malignant phenotype, Cancer Cell 8(3) (2005) 241–54. [PubMed: 16169468]

[5]. Paszek MJ, Weaver VM, The tension mounts: mechanics meets morphogenesis and malignancy, J Mammary Gland Biol Neoplasia 9(4) (2004) 325–42. [PubMed: 15838603]

[6]. Gorczyca W, Holm R, Nesland JM, Laminin production and fibronectin immunoreactivity in breast carcinomas, Anticancer Res 13(4) (1993) 851–8. [PubMed: 8394677]

[7]. Acerbi I, Cassereau L, Dean I, Shi Q, Au A, Park C, Chen YY, Liphardt J, Hwang ES, Weaver VM, Human breast cancer invasion and aggression correlates with ECM stiffening and immune cell infiltration, Integr Biol (Camb) 7(10) (2015) 1120–34. [PubMed: 25959051]

[8]. Lopez JI, Kang I, You WK, McDonald DM, Weaver VM, In situ force mapping of mammary gland transformation, Integr Biol (Camb) 3(9) (2011) 910–21. [PubMed: 21842067]

[9]. Conklin MW, Eickhoff JC, Riching KM, Pehlke CA, Eliceiri KW, Provenzano PP, Friedl A, Keely PJ, Aligned collagen is a prognostic signature for survival in human breast carcinoma, Am J Pathol 178(3) (2011) 1221–32. [PubMed: 21356373]

[10]. Bredfeldt JS, Liu Y, Conklin MW, Keely PJ, Mackie TR, Eliceiri KW, Automated quantification of aligned collagen for human breast carcinoma prognosis, J Pathol Inform 5(1) (2014) 28. [PubMed: 25250186]

[11]. Levental KR, Yu H, Kass L, Lakins JN, Egeblad M, Erler JT, Fong SF, Csiszar K, Giaccia A, Weninger W, Yamauchi M, Gasser DL, Weaver VM, Matrix crosslinking forces tumor progression by enhancing integrin signaling, Cell 139(5) (2009) 891–906. [PubMed: 19931152]

[12]. Provenzano PP, Inman DR, Eliceiri KW, Knittel JG, Yan L, Rueden CT, White JG, Keely PJ, Collagen density promotes mammary tumor initiation and progression, BMC Med 6 (2008) 11. [PubMed: 18442412]

[13]. Provenzano PP, Eliceiri KW, Campbell JM, Inman DR, White JG, Keely PJ, Collagen reorganization at the tumor-stromal interface facilitates local invasion, BMC Med 4(1) (2006) 38. [PubMed: 17190588]

[14]. Grossman M, Ben-Chetrit N, Zhuravlev A, Afik R, Bassat E, Solomonov I, Yarden Y, Sagi I, Tumor Cell Invasion Can Be Blocked by Modulators of Collagen Fibril Alignment That Control Assembly of the Extracellular Matrix, Cancer Res 76(14) (2016) 4249–58. [PubMed: 27221706]

[15]. Grim JC, Marozas IA, Anseth KS, Thiol-ene and photo-cleavage chemistry for controlled presentation of biomolecules in hydrogels, J Control Release 219 (2015) 95–106. [PubMed: 26315818]

[16]. McLane JS, Ligon LA, Stiffened Extracellular Matrix and Signaling from Stromal Fibroblasts via Osteoprotegerin Regulate Tumor Cell Invasion in a 3-D Tumor in Situ Model, Cancer Microenviron (2016).

[17]. Grossman M, Ben-Chetrit N, Zhuravlev A, Afik R, Bassat E, Solomonov I, Yarden Y, Sagi I, Tumor Cell Invasion Can Be Blocked by Modulators of Collagen Fibril Alignment That Control Assembly of the Extracellular Matrix, Cancer Res 76(14) (2016) 4249–4258. [PubMed: 27221706]

[18]. Artym VV, Swatkoski S, Matsumoto K, Campbell CB, Petrie RJ, Dimitriadis EK, Li X, Mueller SC, Bugge TH, Gucek M, Yamada KM, Dense fibrillar collagen is a potent inducer of invadopodia via a specific signaling network, Journal of Cell Biology 208(3) (2015) 331–350. [PubMed: 25646088]

[19]. Berger AJ, Linsmeier KM, Kreeger PK, Masters KS, Decoupling the effects of stiffness and fiber density on cellular behaviors via an interpenetrating network of gelatin-methacrylate and collagen, Biomaterials 141 (2017) 125–135. [PubMed: 28683337]

[20]. Evans A, Whelehan P, Thomson K, McLean D, Brauer K, Purdie C, Baker L, Jordan L, Rauchhaus P, Thompson A, Invasive breast cancer: relationship between shear-wave elastographic findings and histologic prognostic factors, Radiology 263(3) (2012) 673–7. [PubMed: 22523322]

[21]. Fairbanks BD, Schwartz MP, Bowman CN, Anseth KS, Photoinitiated polymerization of PEG-diacrylate with lithium phenyl-2,4,6-trimethylbenzoylphosphinate: polymerization rate and cytocompatibility, Biomaterials 30(35) (2009) 6702–7. [PubMed: 19783300]

[22]. Schindelin J, Arganda-Carreras I, Frise E, Kaynig V, Longair M, Pietzsch T, Preibisch S, Rueden C, Saalfeld S, Schmid B, Tinevez JY, White DJ, Hartenstein V, Eliceiri K, Tomancak P, Cardona A, Fiji: an open-source platform for biological-image analysis, Nat Methods 9(7) (2012) 676–82. [PubMed: 22743772]

[23]. Goswami S, Philippar U, Sun D, Patsialou A, Avraham J, Wang W, Di Modugno F, Nistico P, Gertler FB, Condeelis JS, Identification of invasion specific splice variants of the cytoskeletal protein Mena present in mammary tumor cells during invasion in vivo, Clin Exp Metastasis 26(2) (2009) 153–9. [PubMed: 18985426]

[24]. Ventura E, Weller M, Macnair W, Eschbach K, Beisel C, Cordazzo C, Claassen M, Zardi L, Burghardt I, TGF-beta induces oncofetal fibronectin that, in turn, modulates TGF-beta superfamily signaling in endothelial cells, J Cell Sci 131(1) (2018).

[25]. Pinner S, Sahai E, PDK1 regulates cancer cell motility by antagonising inhibition of ROCK1 by RhoE, Nat Cell Biol 10(2) (2008) 127–37. [PubMed: 18204440]

[26]. Wilkinson S, Paterson HF, Marshall CJ, Cdc42-MRCK and Rho-ROCK signalling cooperate in myosin phosphorylation and cell invasion, Nat Cell Biol 7(3) (2005) 255–61. [PubMed: 15723050]

[27]. Krakhmal NV, Zavyalova MV, Denisov EV, Vtorushin SV, Perelmuter VM, Cancer Invasion: Patterns and Mechanisms, Acta Naturae 7(2) (2015) 17–28. [PubMed: 26085941]

[28]. Sabeh F, Shimizu-Hirota R, Weiss SJ, Protease-dependent versus -independent cancer cell invasion programs: three-dimensional amoeboid movement revisited, J Cell Biol 185(1) (2009) 11–9. [PubMed: 19332889]

[29]. Eddy RJ, Weidmann MD, Sharma VP, Condeelis JS, Tumor Cell Invadopodia: Invasive Protrusions that Orchestrate Metastasis, Trends Cell Biol 27(8) (2017) 595–607. [PubMed: 28412099]

[30]. Krause M, Dent EW, Bear JE, Loureiro JJ, Gertler FB, Ena/VASP proteins: regulators of the actin cytoskeleton and cell migration, Annu Rev Cell Dev Biol 19 (2003) 541–64. [PubMed: 14570581]

[31]. Wang W, Wyckoff JB, Goswami S, Wang Y, Sidani M, Segall JE, Condeelis JS, Coordinated regulation of pathways for enhanced cell motility and chemotaxis is conserved in rat and mouse mammary tumors, Cancer Res 67(8) (2007) 3505–11. [PubMed: 17440055]

[32]. Philippar U, Roussos ET, Oser M, Yamaguchi H, Kim HD, Giampieri S, Wang Y, Goswami S, Wyckoff JB, Lauffenburger DA, Sahai E, Condeelis JS, Gertler FB, A Mena invasion isoform potentiates EGF-induced carcinoma cell invasion and metastasis, Dev Cell 15(6) (2008) 813–28. [PubMed: 19081071]

[33]. Di Modugno F, Bronzi G, Scanlan MJ, Del Bello D, Cascioli S, Venturo I, Botti C, Nicotra MR, Mottolese M, Natali PG, Santoni A, Jager E, Nistico P, Human Mena protein, a serex-defined antigen overexpressed in breast cancer eliciting both humoral and CD8+ T-cell immune response, Int J Cancer 109(6) (2004) 909–18. [PubMed: 15027125]

[34]. Di Modugno F, Mottolese M, Di Benedetto A, Conidi A, Novelli F, Perracchio L, Venturo I, Botti C, Jager E, Santoni A, Natali PG, Nistico P, The cytoskeleton regulatory protein hMena (ENAH) is overexpressed in human benign breast lesions with high risk of transformation and human epidermal growth factor receptor-2-positive/hormonal receptor-negative tumors, Clin Cancer Res 12(5) (2006) 1470–8. [PubMed: 16533770]

[35]. Pignatelli J, Goswami S, Jones JG, Rohan TE, Pieri E, Chen X, Adler E, Cox D, Maleki S, Bresnick A, Gertler FB, Condeelis JS, Oktay MH, Invasive breast carcinoma cells from patients exhibit MenaINV- and macrophage-dependent transendothelial migration, Sci Signal 7(353) (2014) ra112. [PubMed: 25429076]

[36]. Forse CL, Agarwal S, Pinnaduwage D, Gertler F, Condeelis JS, Lin J, Xue X, Johung K, Mulligan AM, Rohan TE, Bull SB, Andrulis IL, Menacalc, a quantitative method of metastasis assessment, as a prognostic marker for axillary node-negative breast cancer, BMC Cancer 15 (2015) 483. [PubMed: 26112005]

[37]. Oudin MJ, Hughes SK, Rohani N, Moufarrej MN, Jones JG, Condeelis JS, Lauffenburger DA, Gertler FB, Characterization of the expression of the pro-metastatic Mena(INV) isoform during breast tumor progression, Clin Exp Metastasis 33(3) (2016) 249–61. [PubMed: 26680363]

[38]. Oudin MJ, Miller MA, Klazen JA, Kosciuk T, Lussiez A, Hughes SK, Tadros J, Bear JE, Lauffenburger DA, Gertler FB, MenaINV mediates synergistic cross-talk between signaling pathways driving chemotaxis and haptotaxis, Mol Biol Cell 27(20) (2016) 3085–3094. [PubMed: 27559126]

[39]. Wickert LE, Pomerenke S, Mitchell I, Masters KS, Kreeger PK, Hierarchy of cellular decisions in collective behavior: Implications for wound healing, Sci Rep 6 (2016) 20139. [PubMed: 26832302]

[40]. Oudin MJ, Barbier L, Schafer C, Kosciuk T, Miller MA, Han S, Jonas O, Lauffenburger DA, Gertler FB, MENA Confers Resistance to Paclitaxel in Triple-Negative Breast Cancer, Mol Cancer Ther 16(1) (2017) 143–155. [PubMed: 27811011]

[41]. Wang W, Eddy R, Condeelis J, The cofilin pathway in breast cancer invasion and metastasis, Nat Rev Cancer 7(6) (2007) 429–40. [PubMed: 17522712]

[42]. Yamaguchi H, Condeelis J, Regulation of the actin cytoskeleton in cancer cell migration and invasion, Biochim Biophys Acta 1773(5) (2007) 642–52. [PubMed: 16926057]

[43]. Arteaga CL, Johnson MD, Todderud G, Coffey RJ, Carpenter G, Page DL, Elevated content of the tyrosine kinase substrate phospholipase C-gamma 1 in primary human breast carcinomas, Proc Natl Acad Sci U S A 88(23) (1991) 10435–9. [PubMed: 1683701]

[44]. Gupton SL, Riquelme D, Hughes-Alford SK, Tadros J, Rudina SS, Hynes RO, Lauffenburger D, Gertler FB, Mena binds alpha5 integrin directly and modulates alpha5beta1 function, J Cell Biol 198(4) (2012) 657–76. [PubMed: 22908313]

[45]. Nam JM, Onodera Y, Bissell MJ, Park CC, Breast cancer cells in three-dimensional culture display an enhanced radioresponse after coordinate targeting of integrin alpha5beta1 and fibronectin, Cancer Res 70(13) (2010) 5238–48. [PubMed: 20516121]

[46]. Wang K, Wu F, Seo BR, Fischbach C, Chen W, Hsu L, Gourdon D, Breast cancer cells alter the dynamics of stromal fibronectin-collagen interactions, Matrix Biol 60–61 (2017) 86–95.

[47]. Sun Z, Guo SS, Fassler R, Integrin-mediated mechanotransduction, J Cell Biol 215(4) (2016) 445–456. [PubMed: 27872252]

[48]. Miron-Mendoza M, Graham E, Manohar S, Petroll WM, Fibroblast-fibronectin patterning and network formation in 3D fibrin matrices, Matrix Biol 64 (2017) 69–80. [PubMed: 28602859]

[49]. To WS, Midwood KS, Plasma and cellular fibronectin: distinct and independent functions during tissue repair, Fibrogenesis Tissue Repair 4 (2011) 21. [PubMed: 21923916]

[50]. Zollinger AJ, Smith ML, Fibronectin, the extracellular glue, Matrix Biol 60–61 (2017) 27–37.

[51]. Matsumoto E, Yoshida T, Kawarada Y, Sakakura T, Expression of fibronectin isoforms in human breast tissue: production of extra domain A+/extra domain B+ by cancer cells and extra domain A+ by stromal cells, Jpn J Cancer Res 90(3) (1999) 320–5. [PubMed: 10359047]

[52]. Koukoulis GK, Howeedy AA, Korhonen M, Virtanen I, Gould VE, Distribution of tenascin, cellular fibronectins and integrins in the normal, hyperplastic and neoplastic breast, J Submicrosc Cytol Pathol 25(2) (1993) 285–95. [PubMed: 7686813]

[53]. Liao YF, Gotwals PJ, Koteliansky VE, Sheppard D, Van De Water L, The EIIIA segment of fibronectin is a ligand for integrins alpha 9beta 1 and alpha 4beta 1 providing a novel mechanism for regulating cell adhesion by alternative splicing, J Biol Chem 277(17) (2002) 14467–74. [PubMed: 11839764]

[54]. Amin A, Chikan NA, Mokhdomi TA, Bukhari S, Koul AM, Shah BA, Gharemirshamlu FR, Wafai AH, Qadri A, Qadri RA, Irigenin, a novel lead from Western Himalayan chemiome inhibits Fibronectin-Extra Domain A induced metastasis in Lung cancer cells, Sci Rep 6 (2016) 37151. [PubMed: 27849000]

Highlights

- Determine that the initial inhibition to invasion in stiff environments is overcome through Mena and integrin α5 organization of fibronectin
- Demonstrate that *MENA* and *MENA-INV* are upregulated in response to stiffness and EGFR/PLCγ1 signaling
- Identify EDA-fibronectin as responsible for the onset of invasion in high stiffness environments
- Confirm that EDA-fibronectin is increased in primary tumors from patients with invasive breast cancer

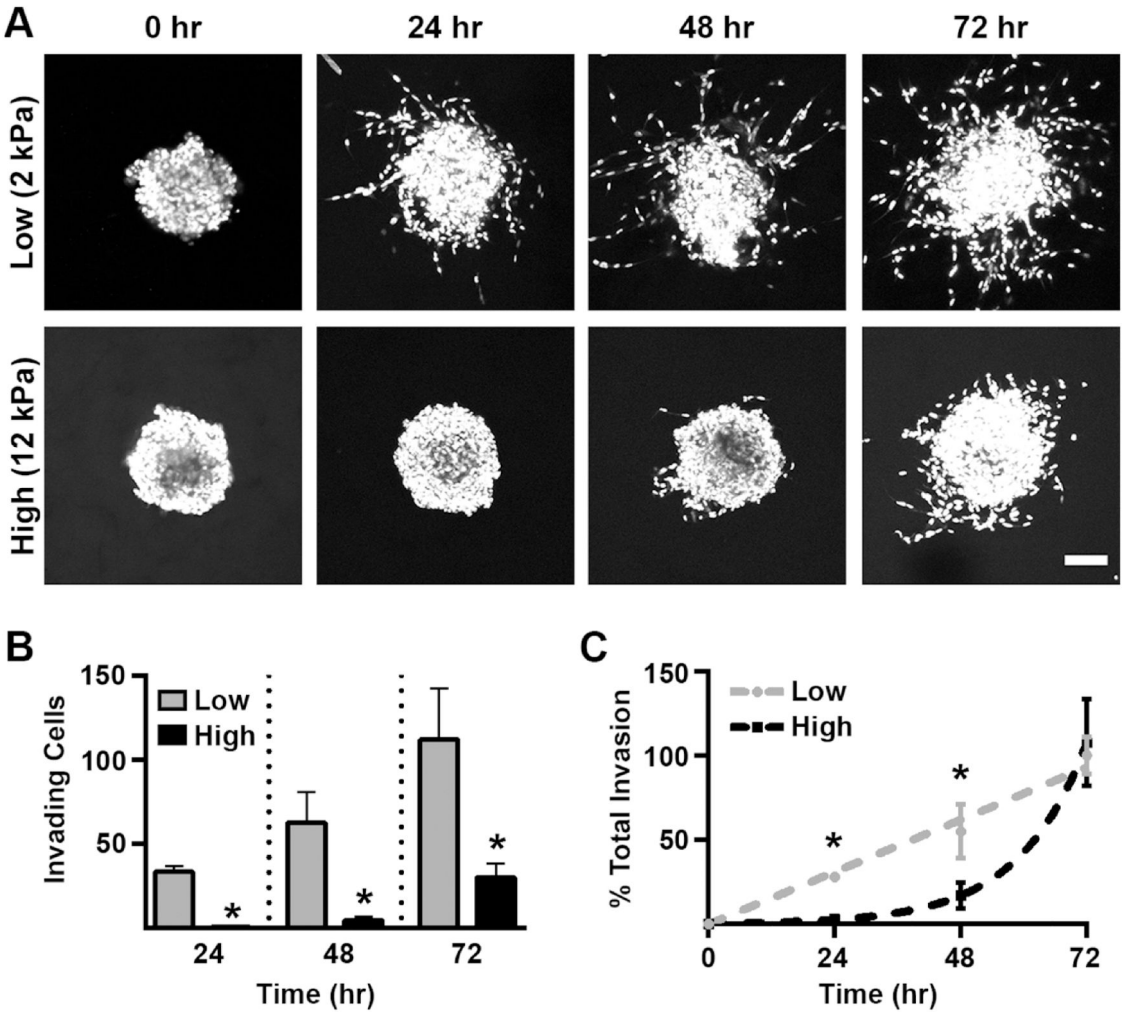

Figure 1:

Scaffold stiffness altered the invasion kinetics of breast cancer spheroids. A.) MDA-MB-231 spheroids were cultured in low and high stiffness gelMA/coll hydrogels for 0, 24, 48, or 72 hours, fixed, and then stained with DAPI to visualize cell nuclei. Shown is a compressed z-stack, scale bar=100 μm. B.) Cell invasion in soft gels occurred sooner and the number of invading cells was greater than in stiffer environments. * denotes $p<0.05$ relative to 2 kPa scaffolds, n=7–14 spheroids per stiffness. C.) The rate of invasion in 2 kPa scaffolds was linear while invasion in 12 kPa gels was delayed and appeared exponential in growth once initiated. * denotes $p<0.05$ relative to 2 kPa scaffolds, n=7–14 spheroids per stiffness.

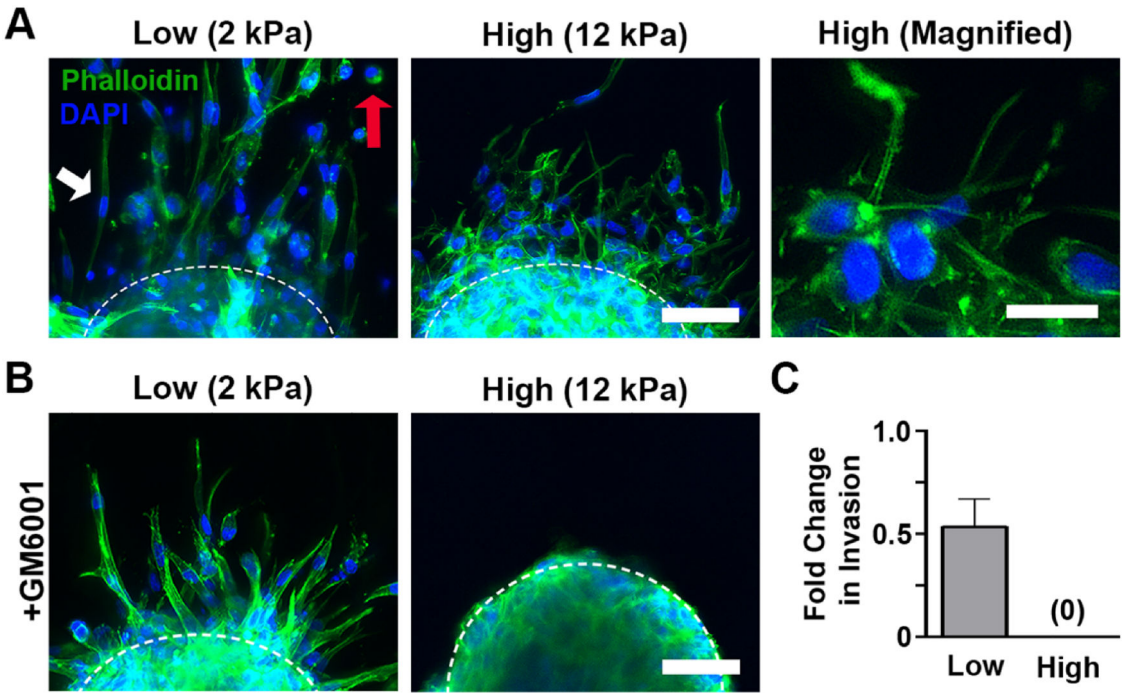

Figure 2:

Morphology and invasion mode differed in low and high stiffness hydrogels. A.) Cells in 2 kPa gels invaded with elongated, symmetrical (white arrow) or amoeboid-like morphologies (red arrow) and few protrusions while those in the 12 kPa conditions developed many actin-enriched protrusions. Scale bar=50 μm (left), 25 μm (right). B.) Addition of GM6001, a pan-MMP inhibitor, did not change morphology in 2 kPa scaffolds, but eliminated the development of actin-enriched protrusions in 12 kPa hydrogels. Scale bar=50 μm. C.) MMP inhibition decreased the amount of cellular invasion at 72 hours in low stiffness gels and completely eliminated invasion when stiffness was increased to 12 kPa. n=11–12 spheroids per condition. In all panels, green is phalloidin and blue is DAPI.

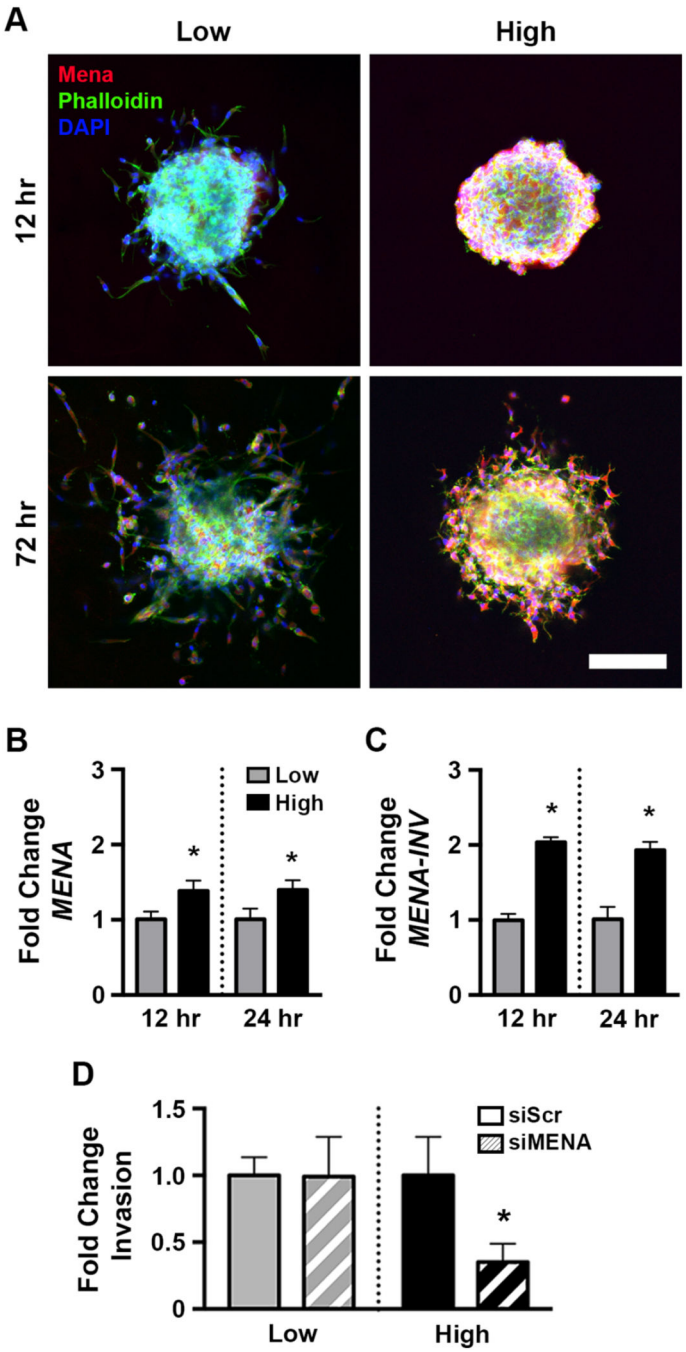

Figure 3:

Increasing stiffness upregulated Mena expression in spheroids, which was necessary for invasion in stiff gels but not soft ones. A) Immunofluorescent staining of spheroids demonstrated Mena upregulation began early and persisted throughout the duration of the experiment. Scale bar=150 μm. Expression of B.) *MENA* and C.) *MENA-INV* was upregulated at 12 and 24 hours in 12 kPa scaffolds compared to the 2 kPa condition. * denotes $p<0.05$ relative to low stiffness at same time point, n=3 pools of >50 embedded spheroids. D.) siRNA knockdown of *MENA* did not affect invasion in soft gels but greatly

reduced it in stiffer conditions. * denotes $p<0.05$ relative to si*Scr* control, n=7–12 spheroids per condition.

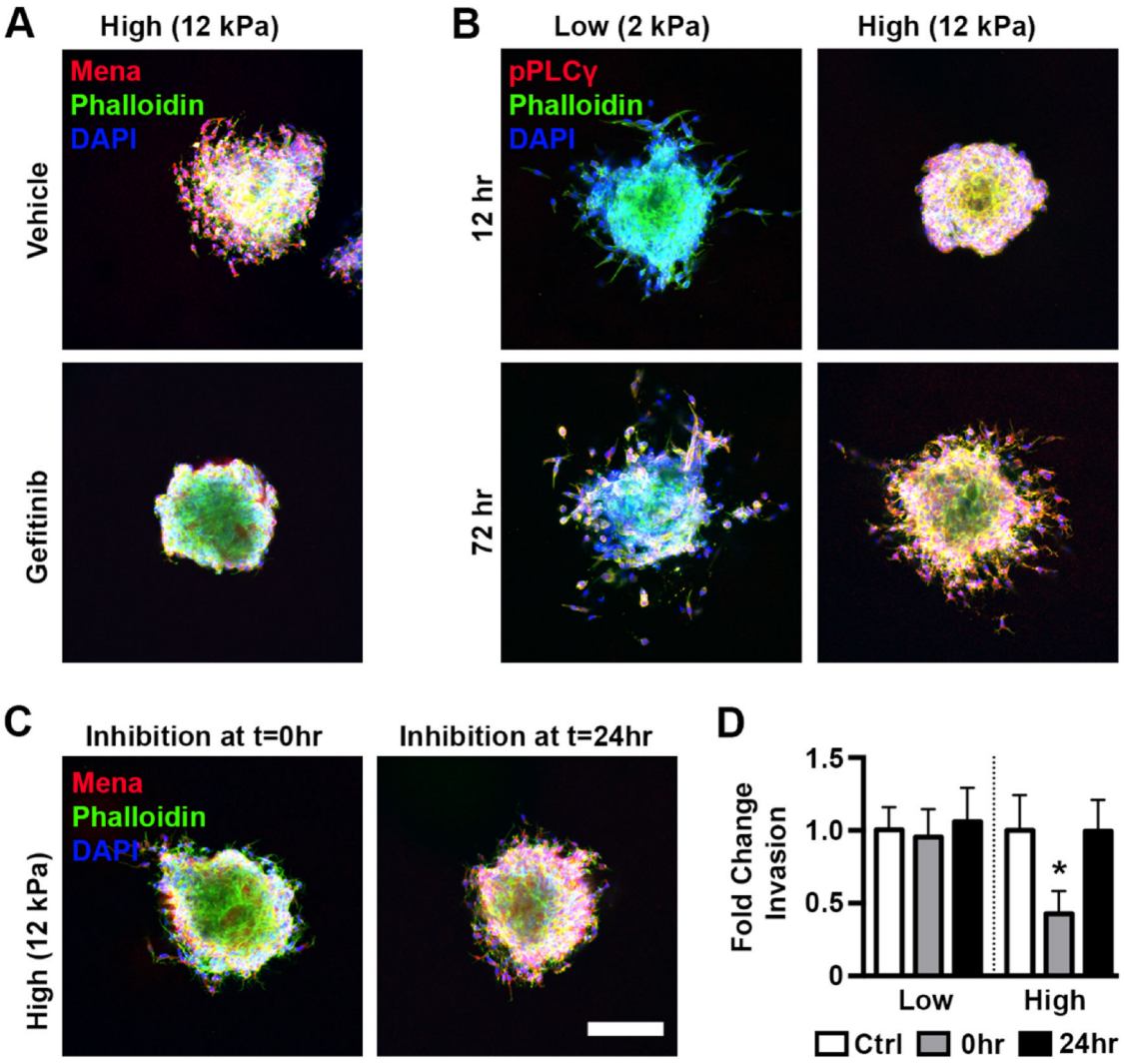

Figure 4:

Mena was upregulated in stiff environments via EGFR activation of PLCγ. A.) Gefitinib treatment of spheroids in 12 kPa gels eliminated invasion and reduced Mena expression around the perimeter of the spheroid. B.) PLCγ1 phosphorylation was increased in stiff gels at both early and late timepoints. C.) Inhibition of PLCγ1 directly after embedding reduced Mena expression while inhibition at 24 hr post embedding had minimal effect. Scale bar=150 μm. D.) PLCγ1 inhibition initiated at 0 or 24 hr did not affect invasion in soft gels, while in stiff gels inhibition initiated at 0 hr but not 24 hr decreased invasion. * denotes $p<0.05$ relative to vehicle control for same stiffness, n=8–13 spheroids per condition.

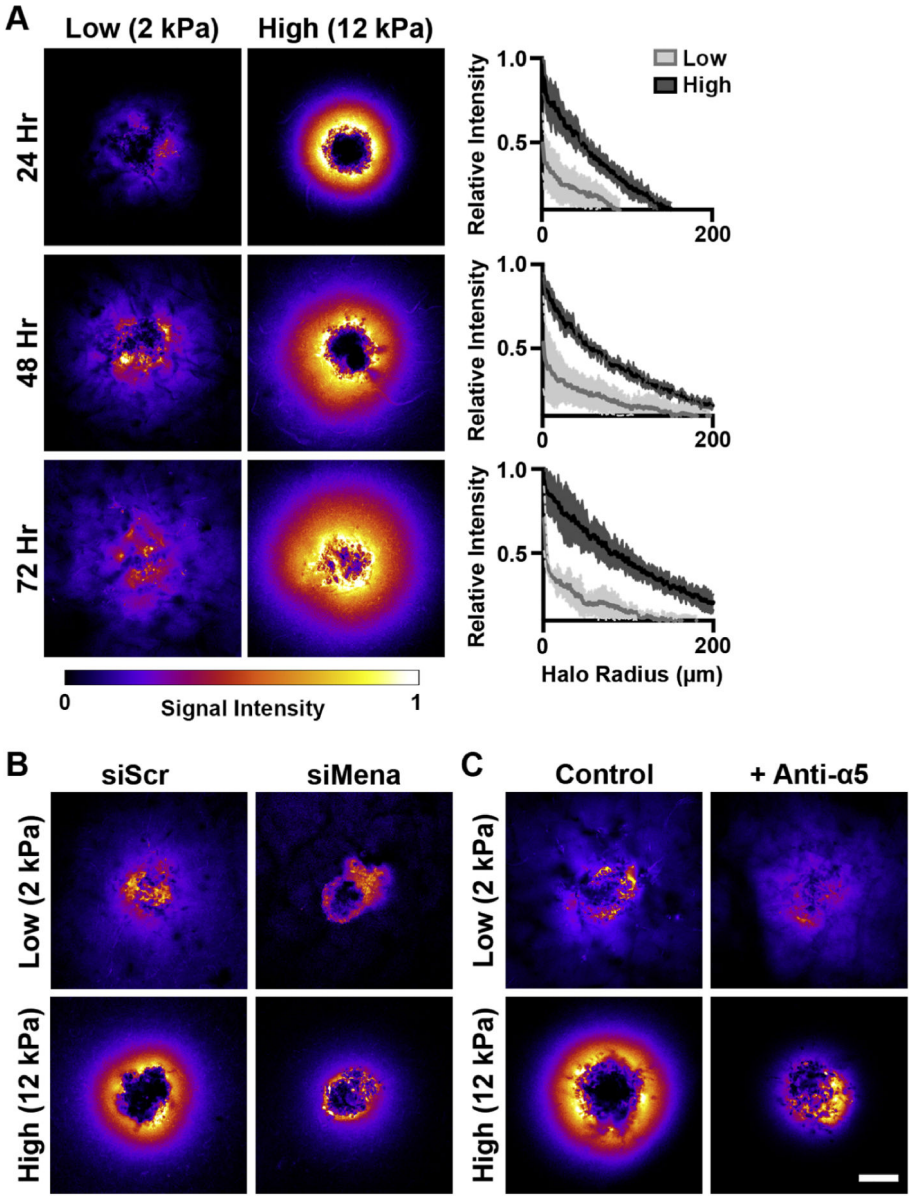

Figure 5:

Fibronectin is enriched around breast cancer spheroids in high stiffness scaffolds due to Mena-mediated assembly. A.) Heatmaps of immunofluorescent staining of fibronectin demonstrated the development of a high intensity halo around spheroids in 12 kPa gels. The halo increased in spread and intensity over time, with clear differences between low and high stiffness conditions. Scale bar=150 μm, solid line is mean and shaded area of line plot is standard deviation, n=3 line intensities per spheroid and 3 spheroids per condition. B.) Heatmaps of fibronectin staining at 24 hr post embedding of spheroids treated with either scrambled (left) or *MENA*-targeted (right) siRNA demonstrated the knockdown of *MENA* decreased the intensity and spread of fibronectin signal. C.) Similarly, fibronectin heatmaps at 24 hr post embedding of spheroids treated with an anti-α5 antibody (right) had reduced intensity and spread of the halo compared to untreated controls (left). Scale bar=150 μm.

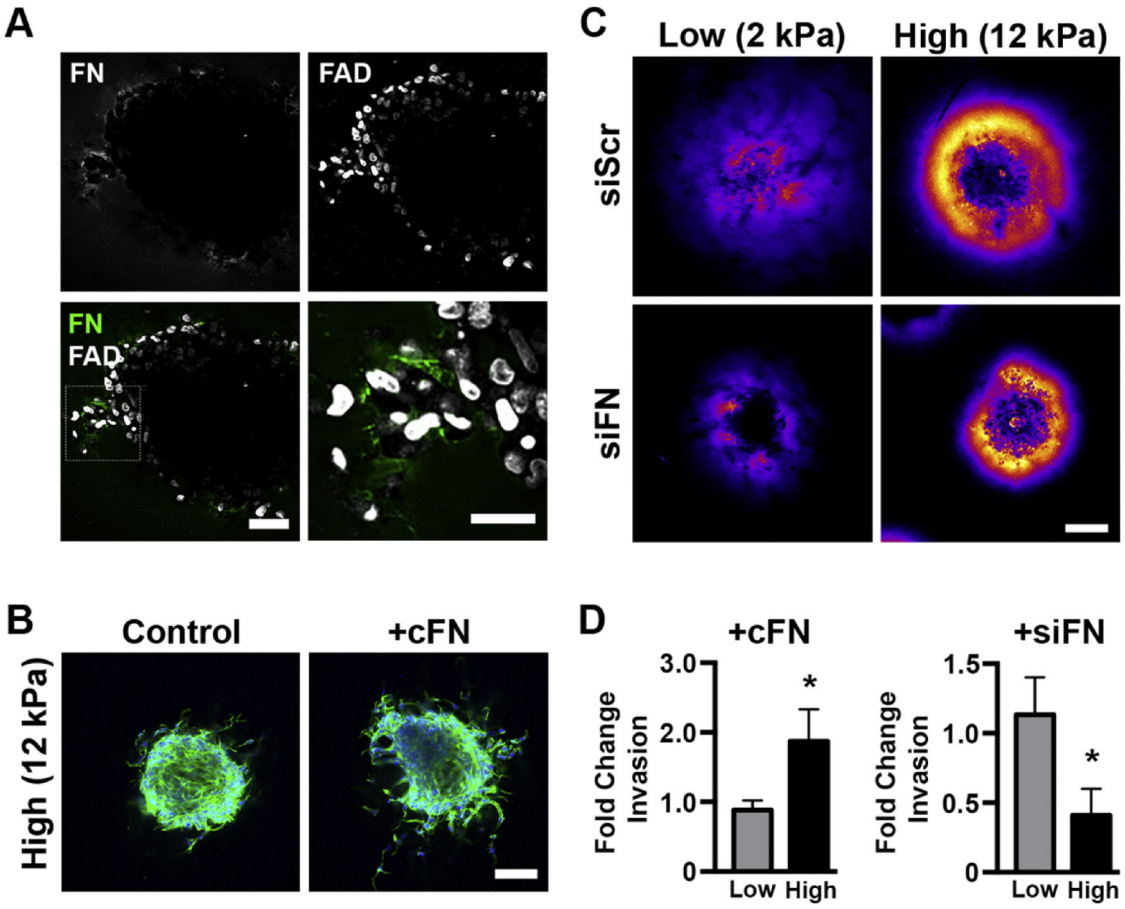

Figure 6:

Increased fibronectin in the local ECM is critical to breast cancer cell invasion in 12 kPa scaffolds. A.) Two-photon microscopy showed increased fibronectin deposition around actively invading cells in spheroids embedded in high stiffness scaffolds. Scale bars=50 and 25 μm (higher magnification of outlined region). B.) The addition of cellular fibronectin to high stiffness gels increased invasion (green is phalloidin, blue is DAPI, scale bar=150 μm), while C.) siRNA knockdown of *FN1* decreased fibronectin intensity and spread in both 2 and 12 kPa gels. Scale bar=150 μm. D.) In high stiffness scaffolds, the addition of cellular fibronectin doubled invasion at 72 hours post embedding while siRNA knockdown of *FN1* drastically decreased invasion over the same period. Neither intervention affected invasion in low stiffness hydrogels. * denotes $p<0.05$ relative to untreated control of same stiffness, n=9–11 and 16–18 spheroids per conditions for the cFN and siFN experiments, respectively.

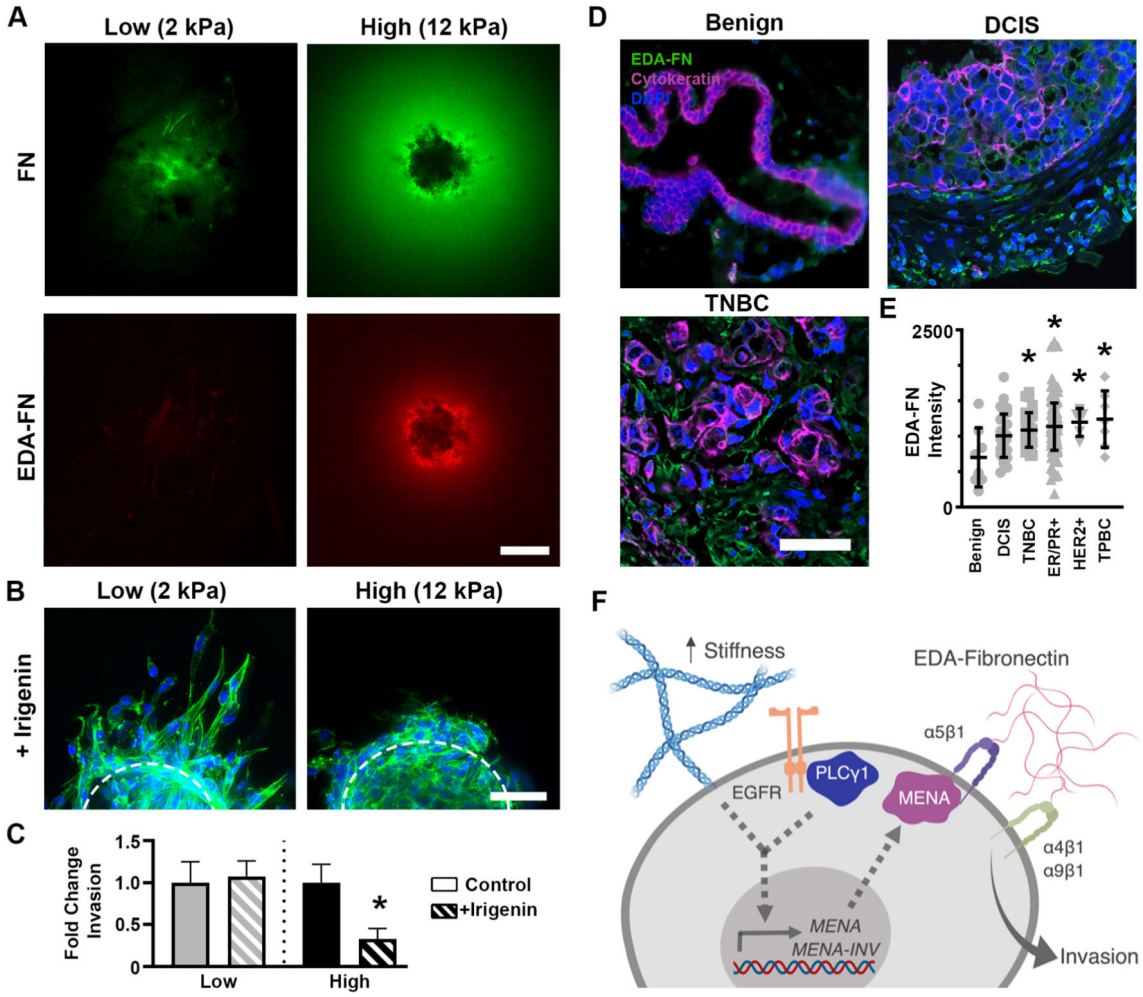

Figure 7:

Local enrichment of EDA-fibronectin drives cell invasion in stiff environments. A.) Total fibronectin and EDA-fibronectin staining in low (left) and high (right) stiffness gels at 72 hr revealed the fibronectin halo that developed in 12 kPa gels consisted of the EDA-fibronectin isoform. Scale bar=150 μm. B.) Treatment with irigenin, a steric blocker of cell-EDA interaction, did not alter morphology in soft conditions but drastically inhibited the invasive morphology in the stiff gels. Scale bar=50 μm. C.) Invasion in high, but not low, stiffness hydrogels was decreased by irigenin treatment. * denotes $p<0.05$ relative to vehicle control for same stiffness, n=15–20 spheroids per condition. D.) Representative image of benign (left), DCIS (middle), and TNBC (right). Green is EDA-FN, pink is pan-cytokeratin, and blue is DAPI. Scale bar = 50 μm. E.) Mean EDA-FN fluorescence levels in benign (n=8), DCIS (n=30), TNBC (n=32), ER/PR+ (n=150), HER2+ (n=5), and TPBC (n=7). Each dot represents an individual patient, bars represent mean and SD. * denotes $p<0.05$ relative to benign samples by Dunnett's test. F.) Summary of stiffness-related invasion mechanism.